Supporting Information: Dynamical Effects and Product Distributions in Simulated CN + Methane Reactions

Thomas J. Preston[1], Balázs Hornung[1], Shubhrangshu Pandit[1], Jeremy N. Harvey[2], and Andrew J. Orr-Ewing[1,*]

[1] *School of Chemistry, University of Bristol, Cantock's Close, Bristol, BS8 1TS, UK.*

[2] *Department of Chemistry, KU Leuven, Celestijnenlaan 200F, B-3001 Leuven (Heverlee), Belgium.*

I. Potential Energy Surface

The diabatic surfaces used to construct the empirical valence bonding (EVB) potential energy surface are composed of additive potential energy terms. Each term describes a specific motion in the molecular complex. All functional forms we use here are identical to our previous work on the Cl + CH_4 → HCl + CH_3 reaction.[1] The functional forms are listed here with the fitted parameters, and are combined with electronic structure calculations of energies at the UCCSD-UHF/aug-cc-pVDZ level, using geometries obtained from modified BB1K/6-31G(d) [see ref. 2] calculations. Full descriptions of the terms are available elsewhere.[1]

a. Functions and Parameters

i. Stretches

Bond stretches are given by Morse functions,

$$E(r_{ij}) = D_0 \left[1 - \exp\left(-\beta\left(r_{ij} - r_{ij,0}\right)\right)\right]^2. \qquad \text{(S1)}$$

Subscripts *i* and *j* denote atom pairs (see Table S1).

Table S1: Stretching Parameters

Species	Stretch	D_0 / kJ·mol^{-1}	$r_{ij,0}$ / Å	β / Å^{-1}
CH_4	C-H	473.0	1.098	1.824
CN	C-N	720.2	1.180	2.617
CH_3	C-H	555.2	1.097	1.781
HCN	H-CN	581.1	1.080	1.802

ii. Bends and Out-of-Plane Motions

Harmonic bends are given by

$$E(\theta_{ijk}) = k_b(\theta_{ijk} - \theta_{ijk,0})^2. \quad \text{(S2)}$$

Subscripts *i*, *j* and *k* denote atoms between which angles are specified (see Table S2) and k_b is the associated quadratic force constant.

Table S2: Bending Parameters.

Species	Bend	k_b / kJ·mol^{-1}·degree^{-2}	$\theta_{ijk,0}$ / degree
CH_4	H-C-H	0.0386	109.47
CH_3	H-C-H	0.0302	120
HCN	H-C-N	0.0176	180

Table S3: Improper (Out-of-Plane) Bending Parameters

Bend	k_b / kJ·mol^{-1}·degree^{-2}	$\theta_{ijk,0}$ / degree
CH_3	0.0157	0.0

iii. van der Waals Interactions

The van der Waals interactions use the following Buckingham-Corner function,[3] with a damping function included as in our CH_4 + Cl work.[1]

$$V(x_{ij}) = \varepsilon_{ij}\left(\frac{8-2c_6}{\beta-8}\exp[\beta_{ij}(1-x_{ij})] - c_6 x_{ij}^{-6} - c_8 x_{ij}^{-8}\right), \quad \text{(S3)}$$

$$x_{ij} = \frac{r_{ij}}{r_{ij,0}},$$

$$c_8 = \frac{6c_6 + \beta - \beta c_6}{\beta - 8},$$

$$f(x_{ij}) = \exp\left[-4(x_{ij} - 1)^3\right].$$

Subscripts *i* and *j* denote atom pairs (see Table S4). The damping function $f(x_{ij})$ is applied for $x_{ij} < 1$.

Table S4: Van der Waals Parameters.

Atom Pair	ε_{ij} / kJ·mol^{-1}	$r_{ij,0}$ / Å	β_{ij}	c_6
C-C	0.87	4.00	8.87	2.91
C-N	0.87	4.00	8.87	2.91
C-H	0.11	3.68	8.80	2.48
N-H	0.11	3.68	8.80	2.48
H-H	0.15	2.96	10.25	3.27

iv. Coupling

The coupling term is a two-dimensional elliptical Gaussian:

$$V_{12}(r_{C-H}, r_{H-CN}) = A \exp\begin{bmatrix} -b_{11}(r_{C-H} - r^*_{C-H})^2 - b_{22}(r_{H-CN} - r^*_{H-CN})^2 \\ -b_{12}(r_{C-H} - r^*_{C-H})(r_{H-CN} - r^*_{H-CN}) \end{bmatrix}, \quad \text{(S4)}$$

$$\begin{bmatrix} b_{11} & \frac{b_{12}}{2} \\ \frac{b_{12}}{2} & b_{22} \end{bmatrix} = \begin{bmatrix} \frac{\cos^2\theta}{2\sigma^2_{\mathrm{C-H}}} + \frac{\sin^2\theta}{2\sigma^2_{\mathrm{H-CN}}} & \frac{\sin 2\theta}{-4\sigma^2_{\mathrm{C-H}}} + \frac{\sin 2\theta}{4\sigma^2_{\mathrm{H-CN}}} \\ \frac{\sin 2\theta}{-4\sigma^2_{\mathrm{C-H}}} + \frac{\sin 2\theta}{4\sigma^2_{\mathrm{H-CN}}} & \frac{\sin^2\theta}{2\sigma^2_{\mathrm{C-H}}} + \frac{\cos^2\theta}{2\sigma^2_{\mathrm{H-CN}}} \end{bmatrix}.$$

The parameters are as follows: *A* is the amplitude of the Gaussian function; r_{C-H} and r_{H-CN} are the H_3C–H and H–CN bond lengths respectively; r^*_{C-H} and r^*_{H-CN} are the coordinates of the centre

of the Gaussian coupling function; $\sigma_{\mathrm{C-H}}$and $\sigma_{\mathrm{H-CN}}$ are the widths of the Gaussian function; and b_{12} defines the angles between the main axis of the coupling term and the r_{C-H} and r_{H-CN} vectors.

Table S5: Coupling Parameters

A / kJ·mol^{-1}	r^{*}_{C-H}/ Å	$\sigma_{\mathrm{C-H}}$/ Å	r^{*}_{H-CN}/ Å	$\sigma_{\mathrm{H-CN}}$/ Å	θ / degree
173.7624	1.28983	1.02745	1.28753	0.615503	151.268

b. Average Error Plot from Final Fit

We perform two distinct checks on the EVB surface relative to the *ab initio* UCCSD-UHF/aug-cc-pVDZ//BB1K/6-31G(d) energies. The first is shown in the main text as Figure 1. The geometries shown therein were not used for fitting, but their EVB and UCCSD energies show remarkable agreement. Here, we show EVB energies minus UCCSD energies from snapshots of trajectories in the top panel of **Figure S1**. The average error is about 4 kJ·mol^{-1}. The bottom panel plots the same data, but as EVB energy versus *ab initio* energy.

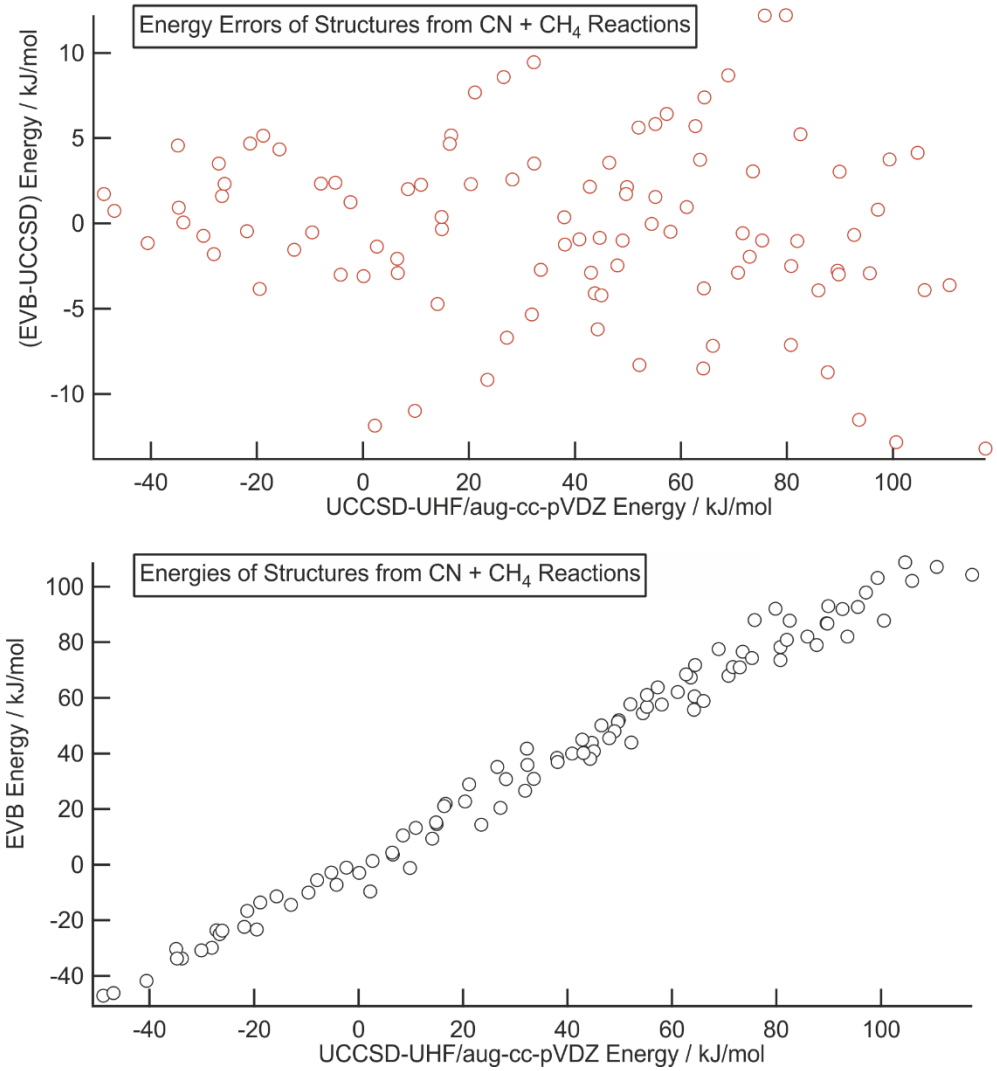

Figure S1. Comparisons of the energies obtained on the EVB surface and the UHF-UCCSD surface for various structures.

c. EVB and NIST Vibrational Frequencies

The harmonic vibrational frequencies of the EVB surface reproduce tabulated vibrational frequencies reliably well. They are listed and compared in **Table S6**.

Table S6. Harmonic Frequencies (in cm^{-1}) of Separated Species in the EVB Fit and from the NIST Webbook.

	CH_4		CD_4	
Mode[a]	EVB[b]	NIST[b]	EVB	NIST
ν_1	2966	2917	2098	2109
ν_2	1489	1534	1053	1092
ν_3	3134	3019	2337	2259
ν_4	1330	1306	998	996
CN				
	EVB	NIST		
	2073	2069		
	CH_3		CD_3	
Mode	EVB	NIST	EVB	NIST
ν_1	3134	3004	2219	2157
ν_2	612	606	476	458
ν_3	3330	3160	2493	2381
ν_4	1385	1400	1017	1026
	HCN		DCN	
Mode	EVB	NIST	EVB	NIST
ν_1	3429	3311	2683	2630
ν_2	690	712	550	569
ν_3	2139	2097	1973	1925

[a] Mode ordering follows NIST Webbook

[b] Energies in cm^{-1}

Table S7 summarizes the harmonic vibrational frequencies of the transition state on the EVB PES.

Table S7: Harmonic Frequencies of the Vibrational Modes of the Transition State on the EVB PES.

Mode Description [a]	Frequency / cm^{-1}
Reaction coordinate	187*i*
Frustrated rotation	91
Frustrated rotation	91
Frustrated rotation	234
Frustrated rotation	234
CH_3 umbrella	1283
C-H* wag	1315
C-H* wag	1315
CH_3 deformation	1449
CH_3 deformation	1449
C-H* stretch	2067
CN stretch	2174
CH_3 symmetric stretch	3026
CH_3 asymmetric stretch	3153
CH_3 asymmetric stretch	3153

[a] H* denotes the transferred H atom.

d. Structure of the Transition State on the EVB PES

Bond lengths and bond angles of the transition state structure on the EVB PES are listed in **Table S8**.

Table S8: Structural Parameters of the Transition State on the EVB PES.

Coordinate [a]	Bond Length / Å
C–H	1.098
H_3C–H*	1.145
H*–CN	1.740
C–N	1.180
	Bond Angle / ^{o}
< H–C–H*	108.4

[a] H* denotes the transferred H atom.

II. Trajectory Analysis

a. Energy distribution plots for CN + CD_4

Cyanide collisions with perdeuterated methane give product distributions that are similar to the CN + CH_4 reactive scattering results presented in the main article. A larger fraction of energy appears in CD_3 vibration and less energy partitions to translational energy, as shown in **Figure S2**. Softer vibrational modes lead to more energy in those modes. Better mass-matching between fragments leads to less energy in TKER. Mean energies in the different degrees of freedom of the products are summarized in **Table S9**.

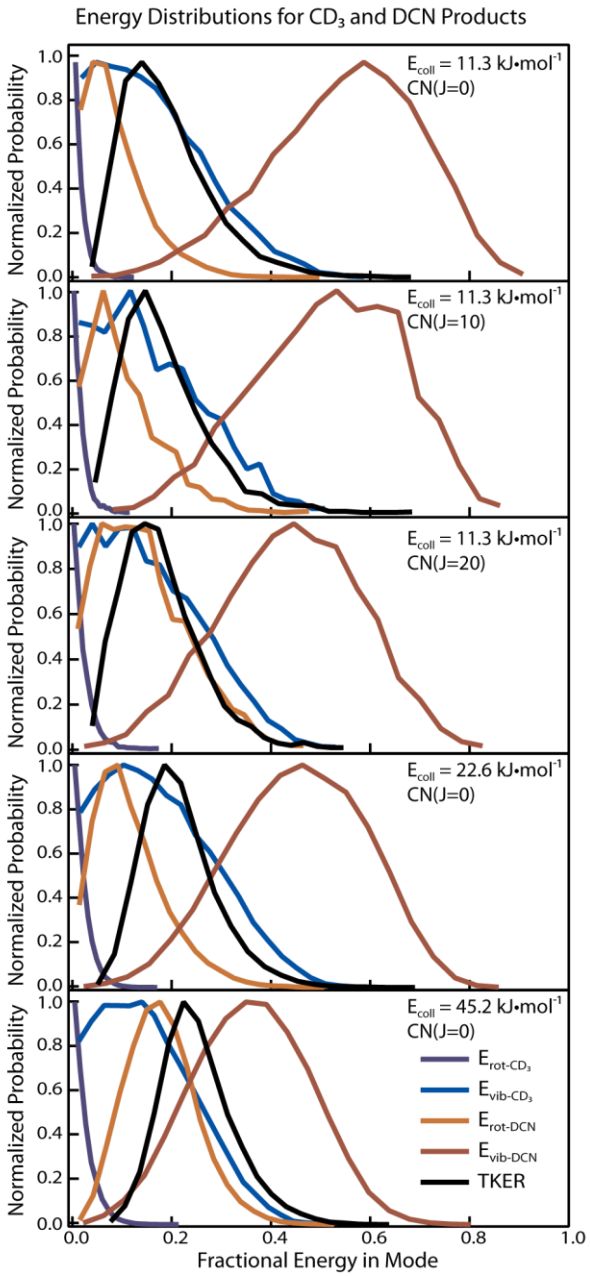

Figure S2. Energy partitioning into CN + CD_4 reaction products. The analysis and description in the main text for CN + CH_4 is applicable to these deuterated results.

Table S9: Collision Energy Dependence of the Mean Energies in the Various Degrees of Freedom of the Products of the CN + CD_4 Reaction.

	Mean Product Energy [a]				
E_{coll} [a]	CD_3 Rotation	CD_3 Vibration	DCN Rotation	DCN Vibration	Kinetic Energy
11.3	1.4	16.3	8.6	55.6	18.9
11.3 (CN *J*=10)	1.7	16.6	10.9	53.7	19.0
11.3 (CN *J*=20)	2.3	17.7	16.1	49.0	19.7
22.6	2.3	19.8	13.1	51.3	24.3
45.2	3.3	20.6	24.4	48.8	34.3

[a] All energies are specified in kJ / mol.

b. Scattering images for CN + CD_4

The scattering images for CN + CD_4 products are remarkably similar to those for CN + CH_4, as shown in **Figure S3.**

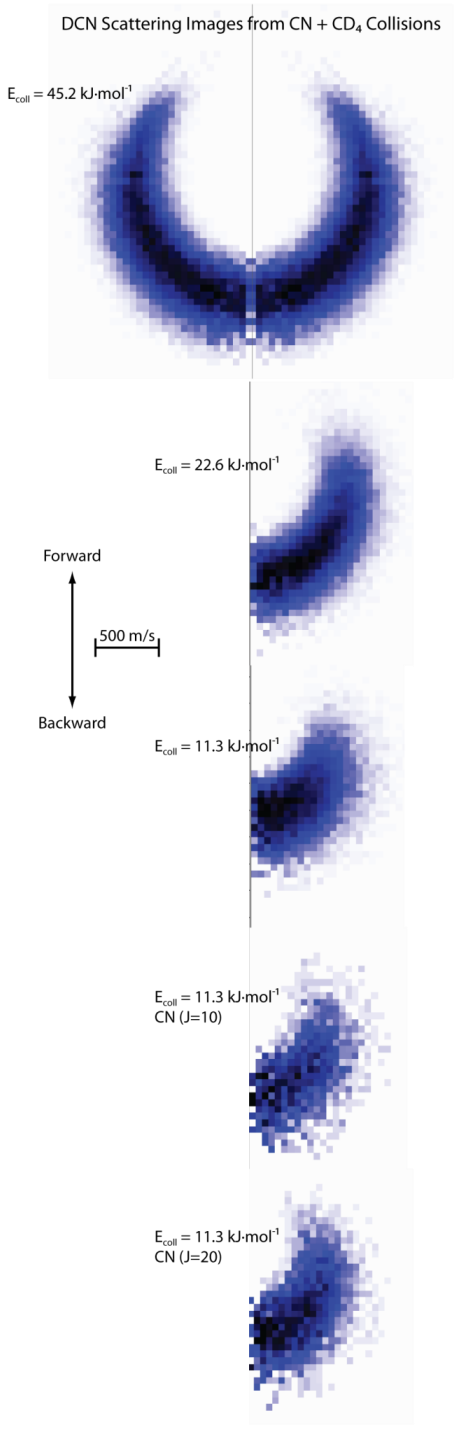

Figure S3. DCN scattering images from CN + CD_4 reactions. The trends in scattering are the same as for CH_4 in the main text.

c. Product Angular Scattering Distributions

The product recoil velocity distributions in the center-of-mass frame are represented as simulated velocity map images in Figure 5 of the main manuscript and Figure S3 of the Supporting Information. In **Figure S4**, we show the dependence of the product scattering angle distributions on collision energy in a more conventional representation.

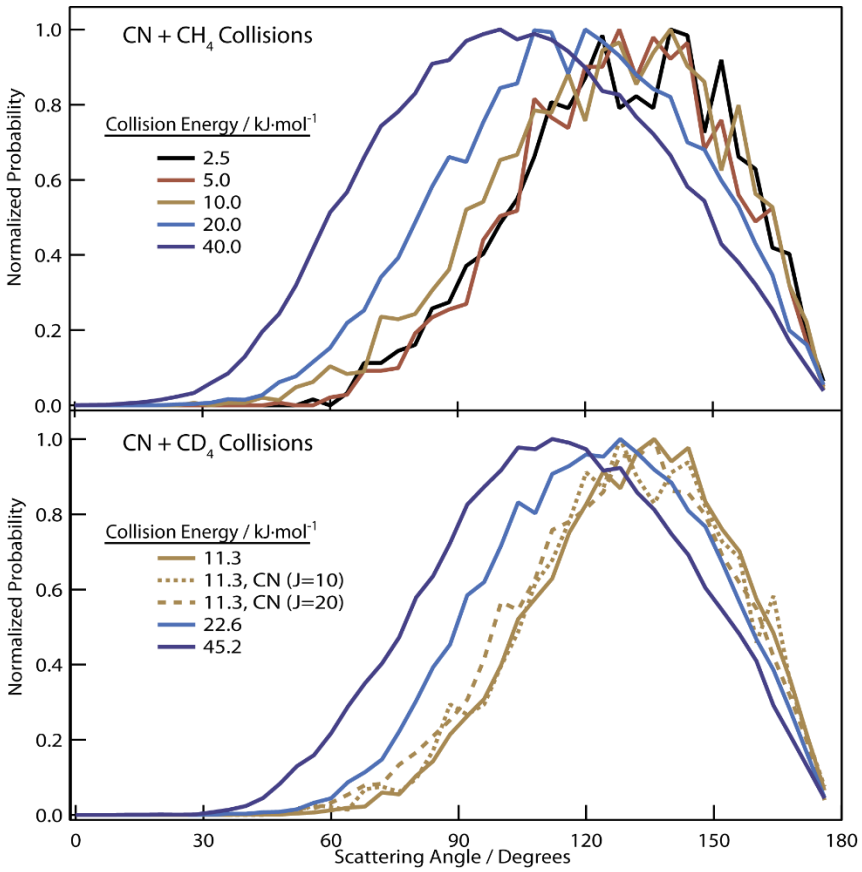

Figure S4: Product scattering angle distributions in the center-of-mass frame for CN + CH_4 (top) and CN + CD_4 (bottom) reactions. The scattering distributions are shown for the different collision energies indicated in the inset keys, and are averaged over all product speeds. In the case of CN + CD_4, the effect of CN rotational excitation is also examined by comparing angular scattering distributions for CN(J=0, 10 and 20) at the same collision energy.

d. Correlation Coefficients for Changing Collision Energies

Many of the correlation coefficients change with collision energy E_{coll}. We show the evolution of some of them in the main text. Here, in **Figure S5**, we show the difference of each correlation coefficient for each collision energy subtracted from the values for E_{coll} = 40.0 kJ/mol.

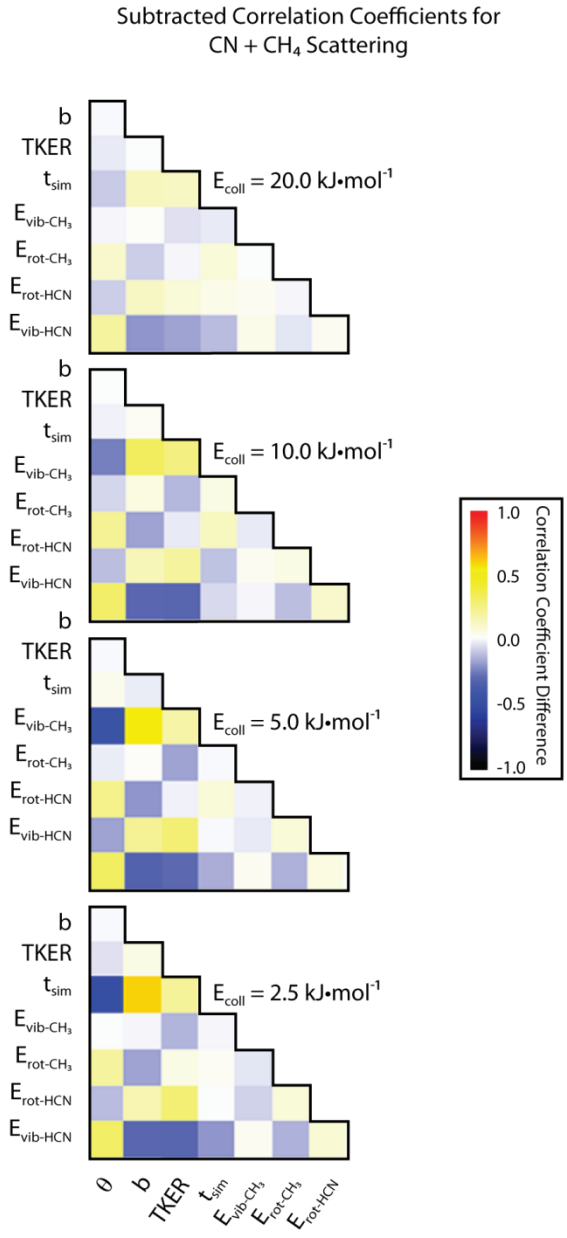

Figure S5. Correlation coefficient differences for CN + CH_4 → HCN + CH_3 reactions. Each value has been subtracted from its value at E_{coll} = 40.0 kJ/mol.

References

1. Hornung, B.; Harvey, J. N.; Preston, T. J.; Dunning, G. T.; Orr-Ewing, A. J. Empirical Valence Bond Theory Studies of the $CH_4 + Cl \rightarrow CH_3 + HCl$ Reaction. *J. Phys. Chem. A* **2015**, *119*, 9590-9598.
2. Glowacki, D. R.; Orr-Ewing, A. J.; Harvey, J. N. Product Energy Deposition of CN + Alkane H Abstraction Reactions in Gas and Solution Phases. *J. Chem. Phys.* **2011,** *134*, 214508.
3. Buckingham, R. A.; Corner, J. Tables of 2nd Virial and Low-Pressure Joule-Thomson Coefficients for Intermolecular Potentials with Exponential Repulsion. *Proc R Soc Lon Ser-A* **1947,** *189*, 118-129.